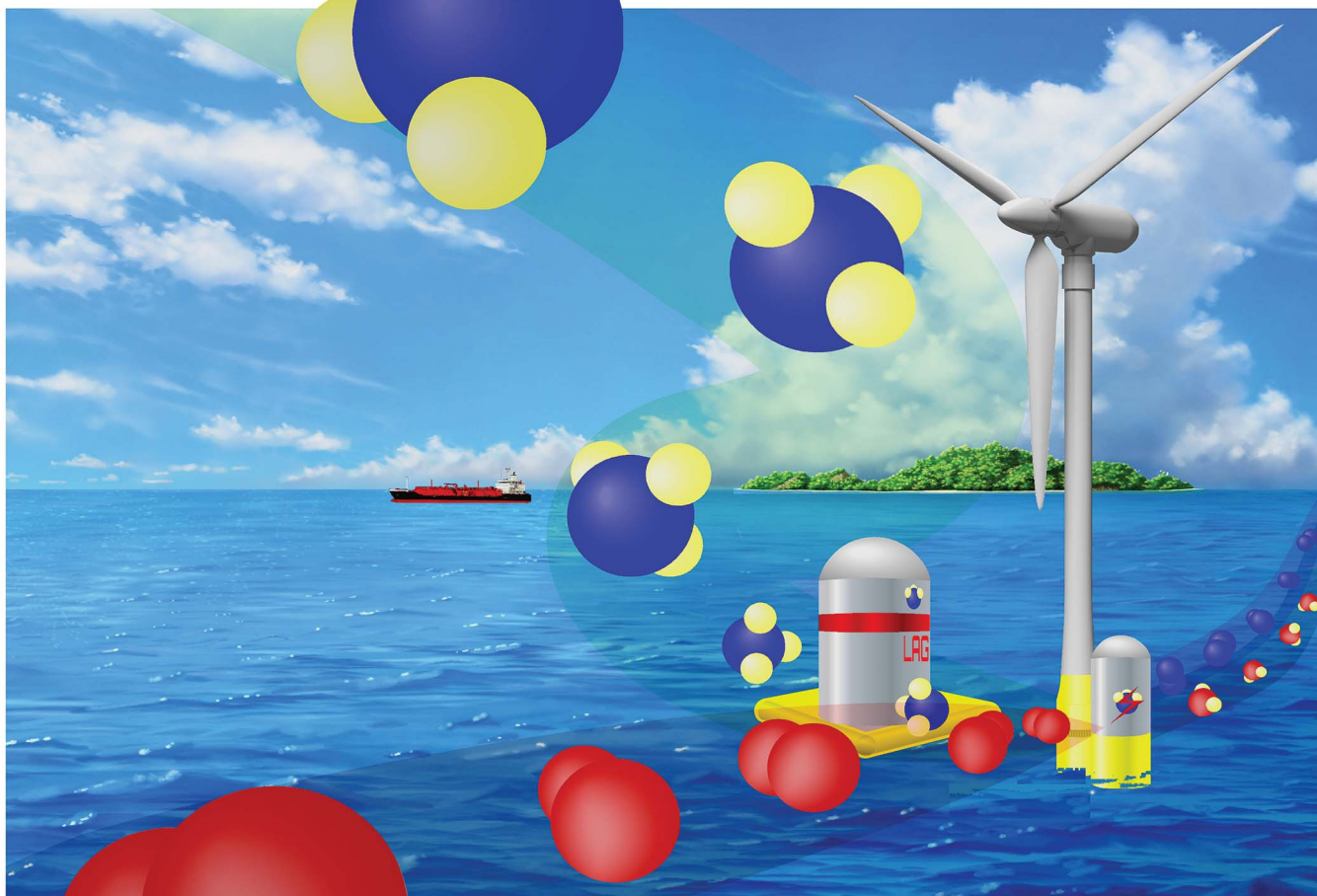


Sustainable Energy & Fuels

Interdisciplinary research for the development of sustainable energy technologies

rsc.li/sustainable-energy



ISSN 2398-4902

PAPER

Jun Kubota *et al.*

Ammonia synthesis from water and nitrogen using electricity with a hydrogen-permeable membrane electrochemical cell with Ru catalysts and molten hydroxide electrolyte: integration with ammonia separation and unreacted gas recirculation



Cite this: *Sustainable Energy Fuels*, 2025, 9, 2658

Ammonia synthesis from water and nitrogen using electricity with a hydrogen-permeable membrane electrochemical cell with Ru catalysts and molten hydroxide electrolyte: integration with ammonia separation and unreacted gas recirculation†

Raisei Sagara, Eriko Watanabe and Jun Kubota  *

There is considerable interest in synthesizing NH_3 directly from abundant H_2O and N_2 using electricity from renewable energy sources, for applications such as synthetic fuels, artificial fertilizers, and raw materials for plastics. NH_3 synthesis from N_2 and H_2O was investigated using an electrochemical setup featuring Ru/Cs⁺/C catalysts, Pd alloy membrane cathodes, NaOH-KOH molten electrolytes, and Ni anodes operated at 250 °C and 1.0 MPa (absolute). This electrochemical setup was integrated with a refrigerated gas/liquid separator at -75 °C to concentrate NH_3 and a recirculation pump for unreacted H_2 and N_2 . As a single-pass reactor, if NH_3 separation and unreacted gas recirculation were not used, this electrochemical device produced NH_3 at 1.0 MPa and 250 °C, with an apparent current efficiency of 32–20% at 10–100 mA cm⁻². This efficiency was limited by the chemical equilibrium, which is calculated to be 36%. The study achieved a 90% apparent current efficiency, with a 320 nmol s⁻¹ cm⁻² production rate of NH_3 at 100 mA cm⁻², 250 °C, and 1.0 MPa with NH_3 separation and unreacted gas recirculation. The remaining 10% of the apparent current efficiency was used for H_2 production. The reaction kinetic properties and scalability of the present system were discussed.

Received 7th March 2025
Accepted 14th April 2025

DOI: 10.1039/d5se00348b
rsc.li/sustainable-energy

1 Introduction

Ammonia (NH_3) is a fundamental chemical substance produced at a rate of 180 million tons per year worldwide, with 85% of it being used as a raw material for chemical fertilizers or directly as a chemical fertilizer to sustain the food supply for humanity.^{1,2} If NH_3 is obtained from renewable energy rather than fossil resources, it can be considered an ideal artificial carbon-free fuel.³ The majority of the NH_3 currently produced is obtained from hydrogen (H_2) derived from fossil resources and nitrogen (N_2) from the atmosphere, typically through a high-temperature, high-pressure chemical process known as the Haber–Bosch process.⁴ It is often stated that NH_3 synthesis uses *ca.* 2% of the human energy consumption.⁵ However, the characterization of NH_3 synthesis as a process with high energy losses because of its high temperature and high pressure is a significant misconception. It is stated that NH_3 has recently been produced at 28–29 GJ ton, which converts to 480 kJ mol⁻¹.^{1,2} NH_3 is an energy-rich chemical substance with a heat of combustion of 382 kJ mol⁻¹,⁶ which is 80% of

consumed energy. In the first place, the synthesis of NH_3 requires 1.5 H_2 , which corresponds to an energy as the heat of combustion of 429 kJ mol⁻¹.⁶ Obtaining H_2 from fossil resources requires additional energy for processes of endothermic reactions such as steam reforming. It is important to recognize that producing H_2 from fossil fuels consumes a significant amount of energy and results in the emission of carbon dioxide (CO_2). Considering this fact, the Haber–Bosch process is extremely efficient in synthesizing NH_3 from H_2 and N_2 , with the energy consumption almost equal to that of the raw material of H_2 .⁷ If high temperature and high pressure are not maintained, efficient heat recovery from the exothermic reaction with high exergy, the ease of liquefaction and separation of NH_3 , and the recycling of unreacted gases will not be possible, resulting in a decrease in process efficiency. It is important to recognize that the process operates at optimal pressure and temperature chosen according to the size of the operation, and while it may involve high temperature and pressure, these factors do not lead to excessive energy consumption. If NH_3 is produced from H_2 originated from fossil resources, the Haber–Bosch process is the most efficient method of NH_3 synthesis that humanity has achieved.

In moving towards establishing a carbon-neutral society without reliance on fossil resources, development of methods to derive the NH_3 needed by humanity from renewable energy

Department of Chemical Engineering, Fukuoka University, 8-19-1, Nanakuma, Jonan-ku, Fukuoka 814-0180, Japan. E-mail: jkubota@fukuoka-u.ac.jp

† Electronic supplementary information (ESI) available. See DOI: <https://doi.org/10.1039/d5se00348b>



sources is essential.⁸ Furthermore, if NH_3 is obtained from renewable energy, it possesses significant value not just as an artificial fertilizer but also as an artificially synthesized fuel.⁹ NH_3 can be synthesized using H_2 obtained from water electrolysis powered by hydropower and N_2 from the atmosphere through the Haber–Bosch process, a method that has been still utilized in some countries worldwide for a long time.² However, instead of the two separate stages of water electrolysis and the Haber–Bosch process, developing a method to directly obtain NH_3 from water and nitrogen using electricity in a single reactor would offer a simpler approach that can better accommodate fluctuating operations. Particularly with the increasing reliance on renewable energies such as solar and wind power, which are variable energy sources rather than hydroelectric energy, establishing processes for fuel production from these power sources is crucially important.^{10,11} Among the various renewable energy sources, photovoltaic, solar thermal, and wind power have the potential to be deployed on a large scale in many regions worldwide, unlike biomass and other sources that are constrained by limited availability.

Various methods have been suggested for the electrochemical synthesis of NH_3 from H_2O and N_2 in the past several years.^{12–18} The important point is to synthesize NH_3 by evolving O_2 from H_2O and N_2 . If NH_3 is synthesized from H_2 and N_2 , it is a downhill exothermic reaction that does not require external energy of electricity; using a catalyst, as in the Haber–Bosch process, allows the reaction to proceed spontaneously without external energy. It must be noted that most of the electrochemical synthesis processes of NH_3 are still in their early stages and far from being practically applicable.^{19,20} One of the most promising approaches seems to be Li-mediated electrochemical synthesis of NH_3 , although it has the drawback of demanding high overpotentials due to reduction to metallic Li.^{21–24} Another promising approach seems to be the application of proton-conducting solid oxide electrochemical cells operating at 400–500 °C.²⁵ However, due to these high temperatures, high pressure like in the Haber–Bosch process is required to have a sufficient conversion ratio in the equilibrium. On the other hand, a huge number of studies have been underway to electrochemically synthesize NH_3 using aqueous solutions and polymer electrolytes at around room temperature, but the reliability of NH_3 production remains uncertain, making industrial application seem unlikely.^{19,20}

The U.S. Department of Energy set numerical targets around 2017 for the development of technology to synthesize NH_3 through an electrochemical pathway, with goals of 300 mA cm^{-2} current density, 90% current efficiency, and 60% energy conversion efficiency.^{10,26} While these values do represent a crucial initial step towards industrial demonstration tests, it should be noted that these benchmarks diverge significantly from the practical characteristics of electrochemical NH_3 synthesis.

In this context, our research group has been conducting studies on an electrochemical device that combines water electrolysis and catalytic NH_3 synthesis for the electrochemical production of NH_3 from H_2O and N_2 , operating within a temperature range of approximately 250 °C. This method aims

to hydrogenate N_2 catalytically, rather than reducing N_2 electrochemically directly. For the electrolysis at 250 °C, phosphate-based electrolytes have been applied.^{27–30} Since phosphoric acid fuel cells (PAFCs) have been successfully commercialized some time ago, there is high potential for the realization of electrochemical devices utilizing phosphoric acid and phosphate electrolytes.^{31–34} The rate of NH_3 production is essentially governed by the chemical equilibrium involving NH_3 , H_2 , and N_2 . Consequently, in synthesis conducted at 250 °C and 1.0 MPa in our previous paper, a maximum of approximately 28% of the current is used for NH_3 production, while the remaining 72% is directed toward H_2 production. The thermodynamic equilibrium limit for current efficiency under these conditions was calculated to be 36%, and the experimental results obtained were almost entirely determined by this equilibrium limitation. This equilibrium limitation is absolute even when using electrochemical methods and cannot be overcome unless a reactor or electrochemical cell capable of separating the produced NH_3 from H_2 and N_2 is employed. While N_2 activation and hydrogenation *via* adsorbed hydrogen atoms migrating on the surface from a hydrogen-permeable membrane can occur, surpassing chemical equilibrium might be possible if an ideal catalyst surface is designed that strongly suppresses H_2 desorption. However, constructing such a surface is not realistic.

Phosphate electrolytes were effectively used for NH_3 synthesis, but increasing the current density led to corrosion issues at the anode. We have achieved stable operation at higher current densities in our electrochemical system using NaOH–KOH molten salt electrolyte at around 250 °C.³⁵ As discussed later in this paper, the NaOH–KOH molten salt becomes a concentrated aqueous solution under humidified conditions and exhibits good ionic conductivity. The most efficient method currently employed by our group for synthesizing NH_3 from N_2 and H_2O involves using Ru catalysts, Pd–Ag hydrogen-permeable membrane cathodes, NaOH–KOH molten salt electrolytes, and Ni anodes at temperatures of 230–250 °C.³⁵ The attempt to electrochemically synthesize NH_3 using molten NaOH–KOH is not the first of its kind. There is an example from a 2014 paper reporting NH_3 production using molten NaOH–KOH at 200–500 °C with an Fe_2O_3 cathode, but the paper was retracted in 2020, likely due to the observation of impurities.^{36–38} The electrolysis using molten NaOH–KOH in this study is not aimed at generating NH_3 by the reduction of N_2 at the cathode/electrolyte interface. It is difficult for gaseous N_2 to penetrate and adsorb at the interface between the cathode and the electrolyte. In the present electrochemical cell, the water electrolysis and NH_3 synthesis sections are separated, and the Ru catalyst provides a clean surface for catalytic reactions at the solid–gas interface. Therefore, this study is completely different from previous research using molten NaOH–KOH, but it is similar in that it attempts to utilize a temperature of around 250 °C.

In situations where a reaction is restricted by equilibrium, a straightforward method to enhance conversion involves the separation of unreacted reactants from the product and their reintroduction into the reaction vessel. This method is employed commonly in various catalytic processes, NH_3 synthesis, methanol synthesis, Fischer–Tropsch synthesis, and



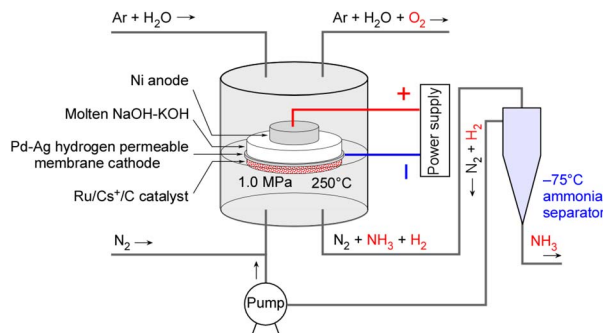


Fig. 1 Schematic diagram of the reaction system in this study.

so on.⁷ This article aims to present our research findings regarding the rate and current efficiency of NH₃ synthesis from H₂O and N₂ through our electrochemical system when integrated with gas-liquid separation and unreacted gas recirculation equipment. Our goal is not to discover a new electrochemical reduction reaction mechanism for N₂, but rather to propose a technology for synthesizing NH₃ efficiently and simply from N₂ and H₂O using electricity.

This paper summarizes the results of investigating the characteristics of NH₃ synthesis using an electrochemical system with NaOH-KOH as the electrolyte and a Ru catalyst for NH₃ synthesis from H₂O and N₂, in which NH₃ separation and unreacted gas recirculation systems were employed. The study aims to demonstrate the potential of this method for practical applications. A schematic diagram of the experimental setup is shown in Fig. 1.

2 Experimental details

2.1. Catalyst preparation

A 30 wt% Ru/Cs⁺/C catalyst (Ru:Cs⁺ = 1:1 molar ratio) weighing 0.25 g was used in the electrochemical cell, placed on the back side of a Pd-Ag membrane cathode. The catalyst was synthesized *via* an impregnation method, where carbon black (Vulcan XC-72R, Cabot Co.) was impregnated with a tetrahydrofuran (THF) solution of Ru₃(CO)₁₂ (TANAKA Kikinzoku Kogyo K. K.) for 4 h with continuous stirring at room temperature. The THF solvent in the carbon black suspension was removed using a rotary evaporator below 40 °C under reduced pressure to prevent the decomposition of the carbonyl complex. The resulting Ru₃(CO)₁₂/C powder was then treated at 400 °C under vacuum to yield the Ru/C catalyst. The addition of the Cs⁺ promoter was carried out by impregnating the Ru catalyst with an aqueous solution of CsNO₃. The Cs⁺-modified Ru/C catalyst was finally treated at 400 °C in a flow of H₂. The state of Cs⁺ compounds was considered to be either CsOH, Cs₂O, or Cs₂CO₃ due to exposure to the atmosphere during storage or impurities during the reaction. However, as this is not definitive, it is referred to as Cs⁺. The detailed procedure can be referenced in our previous paper.^{26–29,33}

The prepared catalyst was observed using a transmission electron microscope (TEM; JEOL JEM-2100F). Additionally,

using a home-built ultra-high vacuum system combined with a quadrupole mass spectrometer, the temperature-programmed desorption (TPD) properties of H₂ from Ru catalysts were investigated. The catalysts were subjected to H₂ reduction treatment at 400 °C and 50 kPa, followed by evacuation at 400 °C, and their H₂ desorption behaviour was measured after adsorption of H₂ at -183 °C and 5.0 kPa.

2.2. Assembly of electrochemical cells

The electrochemical cell used in this study is similar to the one detailed in previous publications,^{27–30,35} as briefly illustrated in Fig. 2A. The cathode was a Pd-Ag membrane with a thickness of 0.1 mm (Pd:Ag = 3:1 in atomic ratio), with a section of the circle with a diameter of 20 mm in contact with the electrolyte. The NaOH-KOH aqueous solution was a mixture of 0.20 mol NaOH, 0.20 mol KOH, and 20 mL H₂O, and *ca.* 5.0 mL of the solution was introduced into the cell. H₂O in the electrolyte was evaporated as the cell was gradually heated to the operating temperature. The anode was a Ni disk with a diameter of 10 mm and a thickness of 5 mm, which was smaller in diameter than the cathode to facilitate the release of generated O₂. The surface of the anode disc was positioned directly facing the cathode, with a separation of about 3 mm between them. The current density in this study was calculated based on the area of the

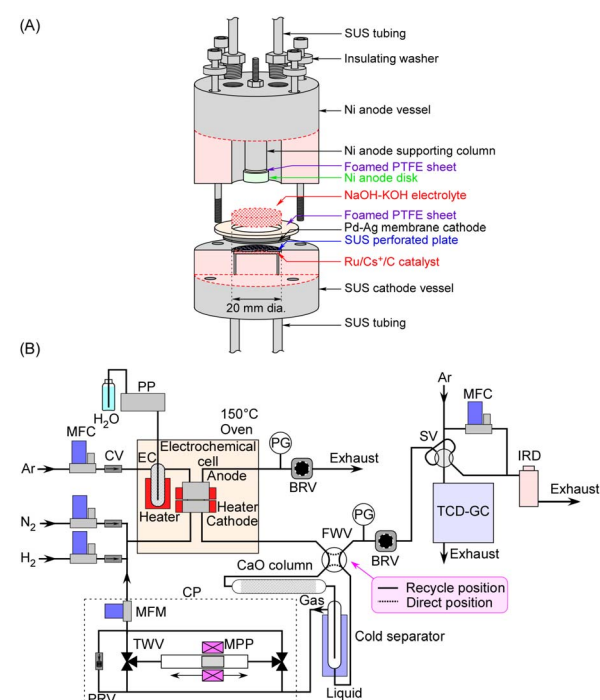


Fig. 2 Detailed cross-sectional view of the electrochemical cell (A) and diagram of the gas lines (B). PP: plunger pump, MFC: mass flow controller, CV: check valve, EC: evaporation chamber, PG: pressure gauge, BRV: back-pressure regulating valve, FWV: four-way valve, CP: circulation pump, MFM: mass flow meter, PRV: pressure relief valve, TWV: electric three-way valve, MPP: magnetic piston pump, SV: sampling valve, TCD-GC: gas chromatograph with a thermal-conductivity detector, and IRD: infrared absorption NH₃ detector.



cathode (3.14 cm^2). Since the sidewall of the anode was also in contact with the electrolyte, it was difficult to accurately define the effective area of the anode.

Our previous paper reported that a polytetrafluoroethylene (PTFE) vessel was used for the anode side while a steel use stainless (SUS) vessel was used for the cathode side,³⁵ to prevent corrosion by the NaOH–KOH molten salt. However, a Ni vessel was employed for the anode side in this work, which exhibited greater mechanical strength than PTFE during operation at $250\text{ }^\circ\text{C}$ and adequately withstood pressurization at 1.0 MPa . The Ni parts of the vessel, except for the anode disc, were electrically insulated, so they did not function as electrodes even when in contact with the electrolyte.

2.3. NH_3 separation and unreacted gas recirculation

The gas lines are depicted in Fig. 2B. Notably, the setup includes a gas–liquid separator and a circulation pump. The gas–liquid separator was mounted on the cold head of a Stirling refrigerator which can be cooled to $-100\text{ }^\circ\text{C}$. For NH_3 separation, the gas–liquid separator was controlled to be at $-75\text{ }^\circ\text{C}$ to prevent the freezing of NH_3 (melting point at $-77.7\text{ }^\circ\text{C}$). The vapor pressure of NH_3 at $-75\text{ }^\circ\text{C}$ is approximately 7 kPa , resulting in an NH_3 concentration of 0.7 vol\% in the recirculated gas during operation at 1.0 MPa , after passing through the gas–liquid separator. For reference, the vapor pressure curve of NH_3 is shown in Fig. S1 in the ESI.†

Inside the gas–liquid separator, liquefied NH_3 accumulates at the bottom of the trap tube, and when the liquid blocks the tube, it is pushed out together with excess N_2 relative to the stoichiometric amount, discharged from the gas–liquid separator, and vaporizes when returning to room temperature. Since NH_3 is not discharged until the liquid blocks the tube is expelled and liquid accumulates again, the NH_3 concentration fluctuates. The average NH_3 concentration over several hours is used to calculate the NH_3 production rate.

The gas–liquid separator has an inner diameter of 4.35 mm , while the liquid discharge tube has an inner diameter of 2.17 mm . The introduction tube to the gas–liquid separator has an outer diameter of 1.58 mm and an inner diameter of 1.0 mm .

To prevent the freezing of water derived from impurities in N_2 from blocking the tube in the gas–liquid separator, the exhaust from the electrochemical cell was passed through a column of quick lime (CaO) to remove moisture.

The circulation pump was custom-built and featured a magnetic piston with an outer diameter of 10 mm . The piston was driven by a reciprocating motion generated by a moving magnet positioned outside the piston cylinder, which was constructed from a nonmagnetic SUS tube. The moving magnet was fixed to a linear stage that reciprocated with a 150 mm stroke, powered by a stepper motor, and provided a displacement capacity of 11.8 cm^3 per stroke. Two electric solenoid-operated 3-port valves were connected to both ends of the piston cylinder, alternating to enable one-way flow. The system was capable of circulating gas at flow rates ranging from 0 to $200\text{ cm}_{\text{STP}}^3\text{ min}^{-1}$ at a pressure of 1.0 MPa . The circulating flow rate was monitored using a mass flow meter (Model 3810DSII,

KOFLOC Corp.). In case of a tubing blockage, a pressure relief valve was installed between the inlet and outlet of the pump to release excess pressure. In this paper, all pressures are expressed as absolute pressures, and gas flow rates are expressed under standard temperature and pressure conditions (STP: $0\text{ }^\circ\text{C}$ and 101.3 kPa).

For unreacted gas recirculation experiments, the exhaust gas from the liquid side of the gas/liquid separator and NH_3 and H_2 productions were quantified using an infrared absorption NH_3 detector with full scales of 1.0 or 15% (Model E12-15, Analytical Technology, Inc. (ATI)) and a gas chromatograph (Model 4200, GL Sciences Inc.) with a thermal conductivity detector, respectively. When the NH_3 concentration exceeded the full scale of the NH_3 detector, the sample gas was diluted with a specified flow rate of Ar before being sent to the NH_3 detector. The exhaust gas from the gas side of the gas/liquid separator was introduced to the cathode side of the electrochemical cell *via* the circulation pump. The gas/liquid separator cannot operate at the exact stoichiometric H_2/N_2 ratio ($=3$) because the liquid NH_3 is pushed out along with the excess N_2 discharged beyond the stoichiometric ratio. Furthermore, along with the discharge of excess N_2 , H_2 is also released with a few % in an apparent current efficiency from the liquid phase side of the separator.

A gas line for H_2 was connected to the cathode side of the cell. However, H_2 was not used for NH_3 synthesis but solely for the pretreatment of the Ru catalyst when installing a fresh catalyst, as well as for conducting a leak test of the system using a portable H_2 detector (Testo 316-2, Testo SE & Co. KGaA).

For single pass experiments, NH_3 was sometimes quantified by absorption of the exhaust gas from the cathode side into $1\text{ mM H}_2\text{SO}_4$ aqueous solutions with monitoring of the electroconductivity, which was used in our previous studies.^{27–30,35}

3 Results and discussion

3.1. Condition of the electrolyte

In this study, since a NaOH–KOH eutectic molten salt was used as the electrolyte, its state will first be explained. An NaOH–KOH (1 : 1 molar ratio) electrolyte was used as a eutectic molten salt with a melting point at $171\text{ }^\circ\text{C}$, which is lower than the operating temperature of the electrochemical cell. The melting points of NaOH and KOH are 318 and $360\text{ }^\circ\text{C}$, respectively, both of which are higher than the operating temperature. Even when the steam supply to the anode side is stopped, the electrolyte remains as a melted eutectic molten salt. However, under the humidified anode gas conditions, the molten salt is considered to become deliquescent by the steam. The anode gas consisted of a mixture of Ar at $10\text{ cm}_{\text{STP}}^3\text{ min}^{-1}$ and liquid H_2O at $5\text{ }\mu\text{L min}^{-1}$, resulting in a steam concentration of 38 vol\% . According to the literature, Henry's law constant for water in NaOH–KOH (63.1 : 36.9 mol%) eutectic molten salt was reported as $0.0095\text{ atm mol}^{-1}\text{ kg}$ at $250\text{ }^\circ\text{C}$. Based on this constant, the amount of H_2O at a total pressure of 0.10 MPa is 40 mol (720 g) per 1 kg of NaOH–KOH melt, and at 1.0 MPa , it is 400 mol (7200 g) per 1 kg of NaOH–KOH melt. While NaOH–KOH is a eutectic molten salt under dry conditions, under the humidified conditions of this experiment, it can be considered



a concentrated aqueous solution. The detailed water concentration in the eutectic molten salt was calculated as shown in Fig. S2 in the ESI.†

3.2. One pass reaction without unreacted gas recirculation

First of all, properties of NH_3 synthesis from N_2 and H_2O using the electrochemical cell without NH_3 separation and unreacted gas recirculation as a function of current density are shown in Fig. 3. NH_3 and H_2 formation rates increased with increasing current density. The apparent current efficiencies (CE) for NH_3 (CE_{NH_3}) and H_2 (CE_{H_2}) formations are defined as follows:^{27–30,35}

$$\text{CE}_{\text{NH}_3}(\%) = \frac{3 \times F \times r_{\text{NH}_3}}{j} \times 100$$

$$\text{CE}_{\text{H}_2}(\%) = \frac{2 \times F \times r_{\text{H}_2}}{j} \times 100$$

where r_{NH_3} and r_{H_2} are electrode area-normalized formation rates of NH_3 and H_2 , respectively, in $\text{mol s}^{-1} \text{cm}^{-2}$. The variable j expresses the current density in A cm^{-2} , and F expresses the Faraday constant of $96\,485 \text{ C mol}^{-1}$. The term “apparent current efficiency” is used because, in this study, the NH_3 synthesis reaction does not involve direct charge transfer to N_2 , but rather

occurs through a hydrogenation reaction by H_2 generated *via* electrolysis. In particular, during the experiment with unreacted gas recirculation, some NH_3 is synthesized from the unreacted H_2 and the current does not directly participate in the recirculation process. Therefore, we refer to it as the “apparent” current efficiency. It represents the efficiency of the current during the overall operation of the system in relation to the rate of NH_3 produced.

The apparent current efficiency for NH_3 formation was 32% at 10 mA cm^{-2} and gradually decreased with increasing current density. On the other hand, the apparent current efficiency for H_2 formation was 66% at 10 mA cm^{-2} and gradually increased with increasing current density. The change in current efficiency for NH_3 formation and H_2 formation as a function of current density is complementary, and their sum is approximately 100%.

As mentioned earlier, the equilibrium limit under these conditions is a current efficiency of 36%, and the NH_3 formation rate and its current efficiency were found to be largely constrained by thermodynamic equilibrium. Apparent current efficiency for NH_3 formation decreased from 32 to 20% on increasing current density from 10 to 100 mA cm^{-2} , and this was due to the insufficient catalyst activity of the Ru catalyst. This is confirmed by the fact that as the current efficiency for NH_3 decreases, the current efficiency for H_2 formation increases. Our previous paper indicated that both the current efficiencies for NH_3 and H_2 formation decreased with increasing current density over 30 mA cm^{-2} . In this study, due to the improved mechanical precision of the cell, up to a current density of 100 mA cm^{-2} , the changes in current efficiency for NH_3 formation and H_2 formation were complementary, and the overall current efficiency was maintained at 100%.

However, when attempting NH_3 synthesis at a current density of 300 mA cm^{-2} , the overall current efficiency deviated significantly from 100%, indicating the occurrence of product cross-leakage. The current efficiency recovers when the current is reduced, so this is not due to irreversible degradation of electrodes and electrolytes, such as electrode corrosion. This could be due to O_2 bubbles generated at the anode interface coming into contact with the Pd–Ag cathode interface, or hydrogen produced at the cathode being unable to be absorbed as H atoms by Pd–Ag and instead generating H_2 gas on the electrolyte side. It is speculated that improvements could be made through the use of separator materials or surface treatment of Pd–Ag, but this will be addressed in future research and development. Although the overall current efficiency was operated at nearly 100% at a current density of 100 mA cm^{-2} , which is one-third of the DOE target in 2017 of 300 mA cm^{-2} , this is considered a promising value for achieving the DOE target.^{10,26}

Next, the dependency on the N_2 flow rate at 100 mA cm^{-2} , 1.0 MPa , and $250 \text{ }^\circ\text{C}$ was examined, as shown in Fig. 4. The current efficiency for NH_3 formation reached a maximum at an N_2 flow rate of around $5\text{--}10 \text{ cm}_{\text{STP}}^3 \text{ min}^{-1}$. In contrast to the behavior observed for NH_3 formation, the apparent current efficiency for H_2 formation decreased at an N_2 flow rate of around $5\text{--}10 \text{ cm}_{\text{STP}}^3 \text{ min}^{-1}$, thus maintaining the total current efficiency at 100%. The stoichiometric N_2 flow rate for 100 mA

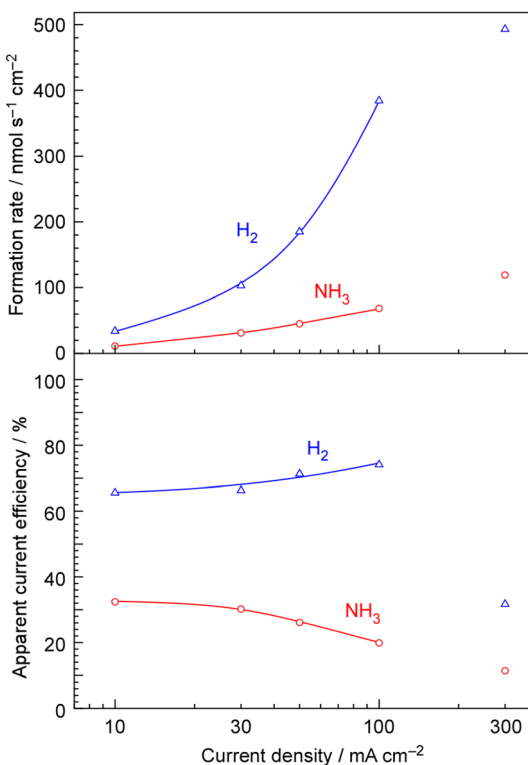


Fig. 3 Formation rates of NH_3 and H_2 , and apparent current efficiency for NH_3 and H_2 formation from H_2O and N_2 at $250 \text{ }^\circ\text{C}$ and 1.0 MPa as a function of current density for one-pass experiments without NH_3 separation and unreacted gas recirculation. The anode gas was a mixture of Ar at $10 \text{ cm}_{\text{STP}}^3 \text{ min}^{-1}$ with $5 \mu\text{L min}^{-1}$ of liquid H_2O . The feeding rate of N_2 was set at $0.10 \text{ cm}_{\text{STP}}^3 \text{ min}^{-1}$ per 1 mA cm^{-2} and was adjusted in proportion to the current density.



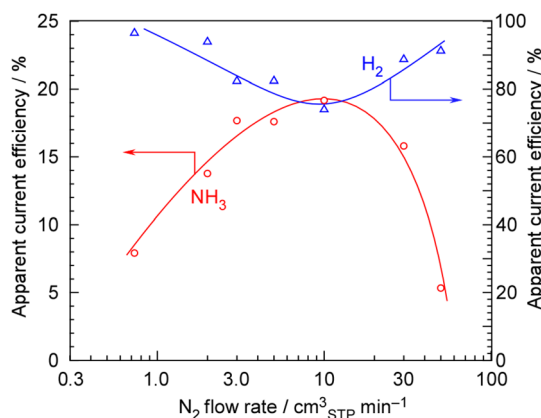


Fig. 4 Apparent current efficiency for NH_3 and H_2 formation from H_2O and N_2 at $250\text{ }^\circ\text{C}$ and 1.0 MPa as a function of the N_2 flow rate for one-pass experiments without NH_3 separation and unreacted gas recirculation. The anode gas was the mixture of Ar at $10\text{ cm}_{\text{STP}}^3\text{ min}^{-1}$ with $5\text{ }\mu\text{L min}^{-1}$ of liquid H_2O .

cm^{-2} is $0.729\text{ cm}_{\text{STP}}^3\text{ min}^{-1}$, meaning that the optimum N_2 flow rate was roughly estimated to correspond to an $\text{H}_2/\text{N}_2 = 0.3$. In our previous paper, the optimum N_2 flow rate was found to be $\text{H}_2/\text{N}_2 = 0.07$ under the conditions of 3.2 mA cm^{-2} , 0.1 MPa , and $250\text{ }^\circ\text{C}$.²⁹ In the present experiment, the optimal N_2 flow rate conditions also deviated significantly from the stoichiometric $\text{H}_2/\text{N}_2 = 3$, with the highest current efficiency for NH_3 formation being achieved where N_2 was in great excess. The reason why these N_2 -excess conditions are optimal for the NH_3 synthesis rate is that, in NH_3 synthesis reactions using Ru-based catalysts, the reaction order with respect to the partial pressure of H_2 is generally negative.^{39,40} In other words, in NH_3 synthesis from the stoichiometric ratio of $3\text{H}_2 + \text{N}_2$, even though H_2 is a reactant, the reaction rate decreases as the partial pressure of H_2 increases. Therefore, the NH_3 formation rate reaches its maximum under conditions where N_2 is in excess.

3.3. Reaction with NH_3 separation and unreacted gas recirculation

The results of NH_3 synthesis from H_2O and N_2 at 30 and 100 mA cm^{-2} with NH_3 separation at $-75\text{ }^\circ\text{C}$ and unreacted gas recirculation are shown in Fig. 5 and 6, respectively. Formation rates of NH_3 and H_2 , the NH_3 concentration at the outlet of the liquid side of the separator, and apparent current efficiency for NH_3 and H_2 formation are plotted against the feeding flow rate of N_2 for each graph. The operation temperature and pressure were $250\text{ }^\circ\text{C}$ and 1.0 MPa .

Fig. 5 (30 mA cm^{-2}) shows that the formation rate of NH_3 gradually increased with the decreasing flow rate of N_2 . In contrast, the formation rate of H_2 gradually increased with the decreasing flow rate of N_2 . The stoichiometric flow rate of N_2 is $0.219\text{ cm}_{\text{STP}}^3\text{ min}^{-1}$ for 30 mA cm^{-2} , so the minimum N_2 flow of $0.50\text{ cm}_{\text{STP}}^3\text{ min}^{-1}$ was 2.3 times. Below a N_2 flow of $1.0\text{ cm}_{\text{STP}}^3\text{ min}^{-1}$, the formation rate of NH_3 became maximum and constant, while the formation rate of H_2 became minimum and constant. The absolute accuracy of the formation rate of H_2 was

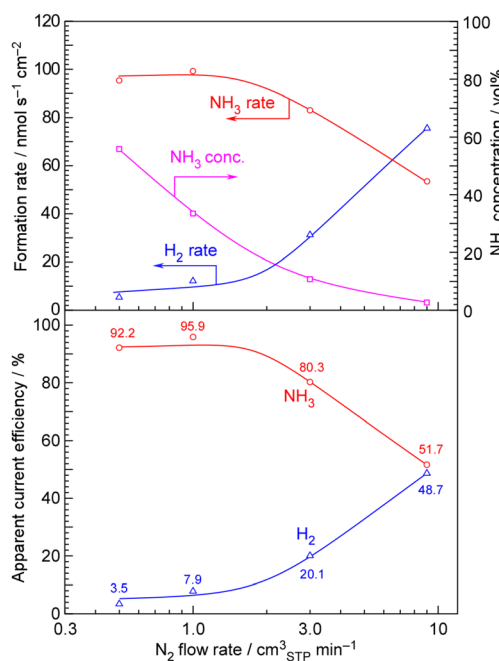


Fig. 5 NH_3 and H_2 formation rates, NH_3 concentration in the exhaust gas, and apparent current efficiency for NH_3 synthesis and H_2 formation from H_2O and N_2 at $250\text{ }^\circ\text{C}$ and 1.0 MPa as a function of the N_2 flow rate, with NH_3 separation at $-75\text{ }^\circ\text{C}$ and unreacted gas recirculation. The current density was 30 mA cm^{-2} and recirculation flow rate was $150\text{ cm}_{\text{STP}}^3\text{ min}^{-1}$. The stoichiometric flow rate of N_2 is $0.219\text{ cm}_{\text{STP}}^3\text{ min}^{-1}$ for 30 mA cm^{-2} . The anode gas was provided from the mixture of Ar at $10\text{ cm}_{\text{STP}}^3\text{ min}^{-1}$ with $5\text{ }\mu\text{L min}^{-1}$ of liquid H_2O .

higher than that of NH_3 ; the apparent current efficiency for the NH_3 formation was estimated to be 94% after subtracting the apparent current efficiency for the H_2 formation about 6% from 100% .

On the other hand, at a current density of 100 mA cm^{-2} as shown in Fig. 6, the apparent current efficiency for H_2 formation was evaluated to be approximately 10% when the N_2 flow rate was below $3.0\text{ cm}^3\text{ min}^{-1}$, so the apparent current efficiency for NH_3 formation was evaluated to be 90% . At any N_2 flow rate and current density, the current efficiencies for NH_3 and H_2 formations add up to approximately 100% , indicating that there is almost no current loss and that either NH_3 or H_2 is being generated.

The total current efficiency may deviate by a few percent from 100% , but this is considered experimental error. NH_3 and H_2 are analyzed using an infrared detector and gas chromatography, and these measurements are quantified relative to the N_2 flow rate. We frequently calibrate the N_2 flow rate as much as possible and conduct experiments carefully to avoid gas leakage, but experimental errors of a few percent to around 10% relative to 100% are unavoidable.

One important point here is that the optimal N_2 flow rate differs significantly from $5\text{--}10\text{ cm}_{\text{STP}}^3\text{ min}^{-1}$ shown in Fig. 4 for a single-pass system without recirculation. Fig. 4 shows the optimal flow rate for achieving the maximum NH_3 formation rate from a kinetic standpoint in a single-pass system. However, the optimal flow rate in a system that combines NH_3 separation



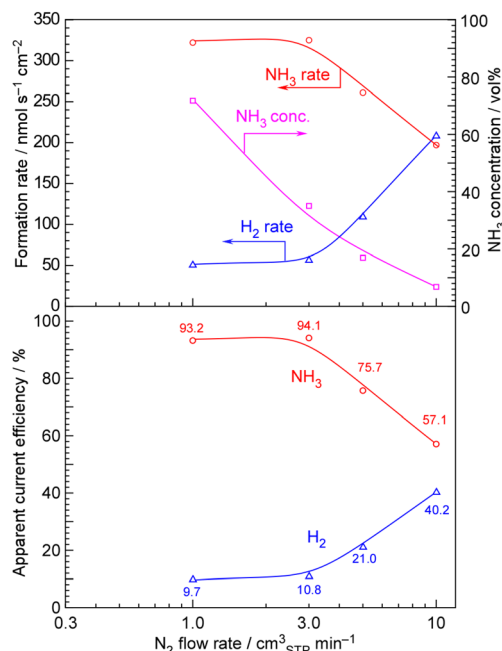


Fig. 6 NH_3 and H_2 formation rates, NH_3 concentration in the exhaust gas, and apparent current efficiency for NH_3 synthesis and H_2 formation from H_2O and N_2 at $250\text{ }^\circ\text{C}$ and 1.0 MPa as a function of the N_2 flow rate, with NH_3 separation at $-75\text{ }^\circ\text{C}$ and unreacted gas recirculation. The current density was 100 mA cm^{-2} and recirculation flow rate was $150\text{ cm}_{\text{STP}}^3\text{ min}^{-1}$. The stoichiometric flow rate of N_2 is $0.729\text{ cm}_{\text{STP}}^3\text{ min}^{-1}$ for 100 mA cm^{-2} . The anode gas was provided from the mixture of Ar at $10\text{ cm}_{\text{STP}}^3\text{ min}^{-1}$ with $5\text{ }\mu\text{L min}^{-1}$ of liquid H_2O .

and unreacted gas recirculation is not determined by kinetics. In a system with NH_3 separation and unreacted gas recirculation, an excess of N_2 , stoichiometrically relative to the H_2 produced by electrolysis, is discharged. In this case, since the system relies on the displacement of liquid NH_3 , the presence of excess N_2 is essential. However, if there is too much N_2 , the system will discharge the unreacted H_2 in nearly 80% current efficiency, along with the excess N_2 . While it is crucial to minimize excess N_2 flow as much as possible in a system with NH_3 separation and unreacted gas recirculation, this suggests that operating in this way is kinetically disadvantageous, as indicated in Fig. 4.

Fig. 7 shows apparent current efficiency for NH_3 and H_2 formation as a function of the recirculation flow rate. Without recirculation (flow rate of 0), the apparent current efficiency for NH_3 formation was 20.0%, and for H_2 formation, it was 74.7%. However, since the horizontal axis of the figure is shown on a logarithmic scale, zero could not be plotted. With the increasing recirculation rate, the apparent current efficiency for NH_3 formation increased in contrast to the decreasing apparent current efficiency for H_2 formation. At any recirculation rate, the current efficiencies for NH_3 and H_2 formations add up to approximately 100%, indicating that there is almost no current loss and that either NH_3 or H_2 is being generated.

Summarizing the results in Fig. 5–7, it was found that keeping the N_2 flow rate below five times the stoichiometric

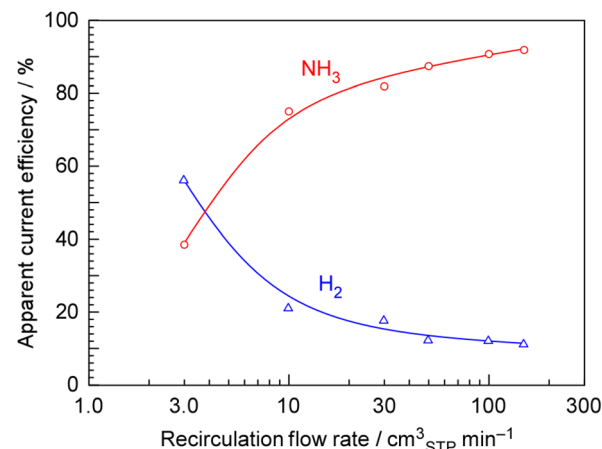


Fig. 7 Apparent current efficiency for NH_3 synthesis and H_2 formation from H_2O and N_2 at $250\text{ }^\circ\text{C}$ and 1.0 MPa as a function of recirculation flow rate, with NH_3 separation at $-75\text{ }^\circ\text{C}$ and unreacted gas recirculation. The current density was 100 mA cm^{-2} and N_2 flow rate was $3.0\text{ cm}_{\text{STP}}^3\text{ min}^{-1}$. The anode gas was the mixture of Ar at $10\text{ cm}_{\text{STP}}^3\text{ min}^{-1}$ with $5\text{ }\mu\text{L min}^{-1}$ of liquid H_2O .

amount and keeping the recirculation rate above 50 times the N_2 flow rate are crucial for achieving an apparent current efficiency of over 90% for NH_3 production.

3.4. Electric properties of electrochemical cells

Time courses of current density and cell voltage are depicted in Fig. 8. In this experiment, electrolysis was conducted by connecting a constant current power supply to the cell to maintain a steady production rate. Therefore, the current remained constant, and the cell voltage fluctuated depending on the conditions of the electrolysis. Fig. 8A shows the cell voltage at current densities ranging from 10 to 300 mA cm^{-2} . Between 10 and 100 mA cm^{-2} , the cell voltage was between 1.5 and 1.8 V . At 300 mA cm^{-2} , the cell voltage was significantly higher at 3 V compared to the cell voltage at 100 mA cm^{-2} or below. Furthermore, the cell voltage was unstable and exhibited significant fluctuations. As seen in the results of Fig. 3, the cell did not function properly at 300 mA cm^{-2} , and the total current efficiency was not 100%.

The inset of Fig. 8A shows the relationship between current density and cell voltage. Despite the instability at 300 mA cm^{-2} , the current density and cell voltage showed an approximately linear relationship. If the activation overpotential of an electrochemical reaction determines the cell voltage, the relationship between current density and cell voltage should follow an exponential curve based on the Tafel equation. However, since the experimental results were linear, it can be concluded that the cell voltage does not depend on the activation overpotential. It is suggested that factors, such as resistance due to the ionic conductivity of the electrolyte, bubble generation, or mass transport, determine the magnitude of the overpotential.

An important factor to consider when evaluating cell voltage is the reduction in energy efficiency caused by overpotential. Table 1 shows thermodynamic parameters for NH_3 synthesis



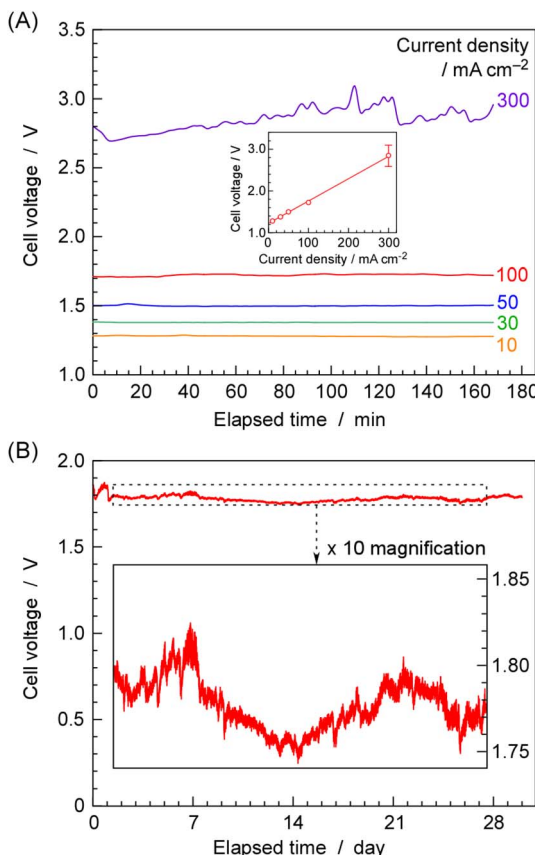


Fig. 8 Time courses of cell voltage at various current densities (A) and cell voltage changes over several weeks of operation at 100 mA cm^{-2} (B) for NH_3 synthesis and H_2 formation from H_2O and N_2 at 250°C . The inset of (A) shows the relationship between current density and cell voltage. The error bar at 300 mA cm^{-2} in (A) represents three times the standard deviation of the data fluctuation.

from H_2O and N_2 . For reference, the values for the electrolysis of H_2O to H_2 and O_2 are also included in Table 1. The energy is presented in kJ mol^{-1} with respect to H_2 and converted to volts based on the corresponding number of electrons. The values are calculated for standard conditions, for liquid water at 25°C , and for steam at temperatures of 25°C and 250°C . The value at 25°C for steam is hypothetical. In the NH_3 synthesis from H_2O and N_2 , the equilibrium potential at 250°C is 1.15 V , and the experimental results were between 1.5 and 1.8 V , which are higher than the equilibrium potential due to the overpotential.

Table 1 Thermodynamic parameters for NH_3 synthesis from H_2O and N_2 and H_2O electrolysis to H_2 and O_2 . The energy is presented in kJ mol^{-1} with respect to mol of H_2

Reaction	Temp. ($^\circ\text{C}$)	H_2O	ΔG_r equilibrium potential		ΔH_r thermoneutral potential	
			$\text{kJ mol}_{\text{H}_2}^{-1}$	V	$\text{kJ mol}_{\text{H}_2}^{-1}$	V
NH_3 synthesis	25	Liq.	226	1.17	255	1.32
	25	Steam	218	1.13	211	1.09
	250	Steam	223	1.15	211	1.09
H_2O electrolysis	25	Liq.	237	1.23	286	1.48
	25	Steam	229	1.19	242	1.25
	250	Steam	218	1.13	244	1.26

In terms of energy efficiency, the voltage efficiency is calculated based on the thermoneutral potential rather than the equilibrium potential, and when multiplied by the current efficiency, it gives the energy efficiency of the electrochemical cell itself. When calculated from liquid water under standard conditions, NH_3 is an energy material with a potential of 1.32 V . This means that a voltage range of 1.5 to 1.8 V corresponds to a voltage efficiency of 88% to 73% . At a current density of 30 mA cm^{-2} , the apparent current efficiency was 94% , and since the electrolytic voltage was 1.7 V , the voltage efficiency was 78% , resulting in an energy efficiency of 73% . Naturally, this energy efficiency does not account for losses due to the evaporation of H_2O , heat loss from NH_3 separation and unreacted gas recirculation, or the heat required for NH_3 liquefaction, and it only represents a very simplified efficiency.

Fig. 8B shows the fluctuation of cell voltage for 100 mA cm^{-2} operation. During the several weeks of experimentation, the cell voltage fluctuated between 1.75 and 1.85 V , but no signs of degradation, such as an increase in cell voltage, were observed.

To investigate whether the cause of increased overvoltage or instability at high current densities lies in the anode or the cathode, it is useful to use a three-electrode cell equipped with a reference electrode to measure the overvoltage of each electrode. In our previous work with phosphate electrolytes, we constructed a three-electrode cell and attempted to measure the overvoltage of each electrode, ultimately identifying the anode as the cause of the increased and unstable cell voltage. Similar experiments should be considered for the current alkali molten salt electrolyte. However, since the electrolyte is in liquid form and conducting three-electrode cell experiments is difficult with our current equipment, we have left this as a subject for future investigation. Additionally, AC impedance measurements were conducted in our previous work with phosphate electrolytes, which proved useful in determining the overvoltage due to the ion conductivity of the electrolyte. For the alkali molten salt electrolyte, however, this remains a future task.

3.5. Catalyst characterization

A brief explanation of the properties of the catalyst used is provided below. A transmission electron microscope (TEM) image of the $30 \text{ wt\%}-\text{Ru/Cs}^+/\text{C}$ ($\text{Cs}^+/\text{Ru} = 1 \text{ mol mol}^{-1}$) catalyst is shown in Fig. 9. In the TEM image, it can be seen that small particles, around a few nanometers in size, are dispersed on the surface of carbon black particles which are approximately

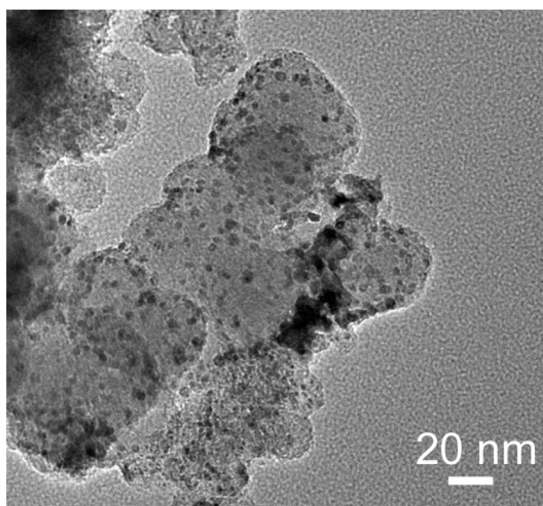


Fig. 9 Transmission electron microscopy image of the 30 wt%-Ru/C ($\text{Cs}^+/\text{Ru} = 1 \text{ mol mol}^{-1}$) catalyst.

40 nm in size. These small particles are identified as Ru particles. The Cs^+ promoter has been added due to its electron-donating effect on the N_2 adsorption sites of Ru, and this electron-donating effect has been clarified through nitrogen adsorption studies using infrared absorption spectroscopy. However, the TEM image does not provide information about the state of Cs^+ .

The effect of addition of alkali-metal compound promoters to Ru catalysts has been extensively discussed using infrared spectroscopic studies on molecularly adsorbed N_2 on Ru sites.^{40–42} Although electronic changes in Ru particles on alkali-metal compound-promoted support materials are difficult to observe using photoelectron spectroscopy, they significantly impact the infrared spectra of molecularly adsorbed N_2 on metallic Ru surfaces.^{40–44} The alkali-metal compound promoters cause a large low wavenumber shift of approximately 300 cm^{-1} in the infrared absorption near 2100 cm^{-1} , which is attributed to the stretching vibration of the $\text{N}\equiv\text{N}$ triple bond in the adsorbed N_2 molecule. When placing a highly electronegative substance, such as an alkali-metal compound, near metal catalyst particles such as Ru, Fe, or Fe, electrons are donated to the metal catalyst particles, making them electron-rich. This electron donation to the anti-bonding orbital, which is the lowest unoccupied molecular orbital (LUMO) of the $\text{N}\equiv\text{N}$ triple bond of the adsorbed N_2 molecule, promotes the dissociation of the adsorbed N_2 .⁴⁵ This explanation has also been commonly cited in describing the function of industrial alkali-metal compound promoters and structure-directing promoters in doubly-promoted Fe catalysts. However, in this study, the effect of adding the Cs^+ compound promoter was examined through H_2 adsorption and desorption studies.

Temperature-programmed desorption (TPD) spectra of H_2 from 30 wt%-Ru/ Cs^+/C ($\text{Cs}^+/\text{Ru} = 1 \text{ mol mol}^{-1}$) and 30 wt%-Ru/C catalysts were measured from -183°C as shown in Fig. 10. The TPD measurement of powder catalysts at low temperatures can be referenced in our previous papers.⁴⁶ For Ru/C,

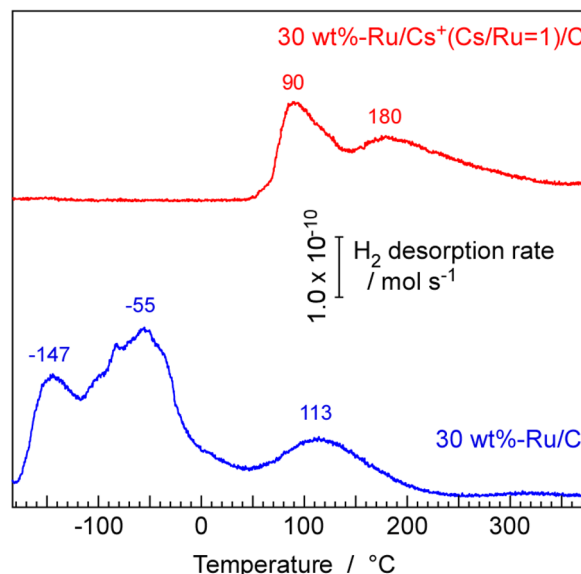


Fig. 10 TPD spectra of H_2 from 30 wt%-Ru/C and 30 wt%-Ru/ Cs^+ ($\text{Cs} : \text{Ru} = 1 : 1$)/C. The ramping rate of temperature was $10^\circ\text{C min}^{-1}$. The samples were treated by reduction treatment at 400°C , followed by evacuation at 400°C , prior to TPD measurements. The adsorption of H_2 was performed at -183°C and 5.0 kPa .

desorption peaks of H_2 were observed at -147 , -55 , and 113°C . From single crystal Ru(0001) surfaces, desorption peaks were reported to appear at 52°C (β_1) and $127\text{--}167^\circ\text{C}$ (β_2).⁴⁷ On the other hand, from Ru(1010) surfaces, a peak was observed at -53°C (α_1).⁴⁸ These peaks are attributed to the desorption through the recombination of dissociatively adsorbed hydrogen atoms. However, this difference is not due to a difference in surface orientation, as the α_1 peak is observed even on Ru(0001) when hydrogen is adsorbed at low temperatures.⁴⁹ In any case, the TPD results obtained under ultra-high vacuum using single-crystal metals show two main peaks: an α peak below room temperature and a β peak at around 100°C . The two low-temperature peaks observed for Ru/C in this experiment are thought to correspond to the α peak, while the high-temperature peak is classified as the β peak. Naturally, since the catalyst used in this experiment is a realistic powder catalyst, there are various effects such as the presence of sites strongly influenced by the support, diverse surface orientations, and crystal edge effects. Therefore, the results are not exactly the same as those obtained with single crystals, but the observed peaks generally correspond to the phenomena observed with single-crystal metals.

A very interesting result is the TPD spectrum from the Ru/ Cs^+/C sample, in which the Cs^+ promoter was added. The low-temperature desorption peak classified as α completely disappeared for Ru/ Cs^+/C . Furthermore, the peak at around 100°C clearly split into two peaks at 90°C and 180°C . In studies conducted on the Ru(0001) surface under ultra-high vacuum, the TPD spectra of H_2 desorption from a surface modified with K metal on Ru(0001) have also been investigated,⁴⁸ but the disappearance of the α peak due to the addition of K has not been reported. Of course, the modification with K in surface



science studies involves partially covering the Ru surface with metallic K, which is entirely different from the addition of Cs^+ compounds as promoters in practical catalysts.

The effect of alkali metal compound promoters has primarily been highlighted in terms of the dissociation process of molecularly adsorbed N_2 , which is the rate-determining step in the NH_3 synthesis reaction. This effect involves the donation of electrons to the adsorbed N_2 through Ru, weakening the bond between nitrogen atoms and promoting dissociation. However, as explained in the previous section, adsorbed hydrogen atoms have an exclusive inhibitory effect on N_2 adsorption. Since the addition of Cs^+ compound is related to the presence of weakly adsorbed hydrogen atoms, it has emerged that this could indirectly affect the rate of the NH_3 synthesis reaction. The effect of additives on the strength of hydrogen adsorption is a new perspective. It has been reported that with certain supports and additives, the hydrogen poisoning effect, the negative reaction order for partial pressure of H_2 in NH_3 synthesis, changes from negative to positive.^{50,51} This may be linked to this effect on hydrogen adsorption by the additives. However, in the case of Ru/ Cs^+ /C in this study, as discussed in Fig. 4, although weakly adsorbed hydrogen atoms were no longer observed in the TPD with Cs^+ addition, hydrogen poisoning still occurred in the NH_3 synthesis reaction and nitrogen-excess conditions were found to favor the reaction.

3.6. Considerations for practical applications

Assuming the operation at 100 mA cm^{-2} and 1.8 V , as achieved in this study, the power density is estimated to be 0.18 W cm^{-2} , which is approximately 0.2 W cm^{-2} . For example, to fully utilize the power generated by typical 2 MW-class wind turbines, which are commonly used as a standard in floating offshore wind farms,^{52,53} the scale of power is 10 million times that of our electrochemical cell. Therefore, it would be necessary to construct an electrochemical system with an electrode area of *ca.* 10 million cm^2 , or 1000 m^2 . This corresponds to 250 stacks of cells with square electrodes measuring 2 m per side. If the thickness of the single cell can be constructed to be within 2 cm, the total thickness of the stack would be less than 5 m. Since the diameter of the tower of a 2 MW-class wind turbine is approximately 5 m, it can be understood that the system can be housed within the tower. Converting the production rate of $320 \text{ nmol s}^{-1} \text{ cm}^{-2}$ obtained in this study to an electrode area of 10 million cm^2 , the production rate becomes 3.2 mol s^{-1} , yielding 54 g s^{-1} of NH_3 , as being produced with a molecular weight of NH_3 of 17 g mol^{-1} . This equates to 190 kg per hour, or 4600 kg per day. It will be possible to produce the amount of NH_3 equivalent to one tank truck with a capacity of 5 tons in one day using a 2 MW-class wind turbine. Although wind turbines in the future are expected to be larger, such as in the 12 MW-class,⁵³ the cells will also become larger accordingly. Of course, this calculation is a simplified one that ignores the power required for N_2 separation from the air, NH_3 separation, refrigeration for unreacted gas recirculation, and pump power. However, these energy requirements are smaller compared to the energy needed to produce H_2 by water splitting, so the NH_3 production rate will not be reduced by half.

If we calculate the price of NH_3 produced at the current electricity rates, it turns out to be significantly more expensive than NH_3 produced from natural gas, making this calculation meaningless. However, if surplus renewable energy, which cannot be connected to the power grid, becomes available in the future, it might be important to convert it into NH_3 in this way and use it as fuel for power generation or transportation equipment.

The electrochemical system in this study is not in its final form. Since it uses a large amount of expensive and rare Pd, there is a need to reduce its usage. Even for the Ru catalyst, which is also rare, alternative catalysts are necessary. The efficiency of NH_3 liquefaction and separation also needs to be improved to reduce energy losses. The current density of 100 mA cm^{-2} needs to be increased by at least several times, and if this is achieved, the system could be made smaller. Additionally, although there was no degradation after about 1 month of operation, longer term stability must also be investigated, and issues such as electrolyte evaporation need to be examined. Moreover, when scaling up, it is essential to ensure that the same performance is maintained. There are many challenges that must be addressed, but we would like to propose this method as the simplest approach for synthesizing NH_3 from H_2O and N_2 using electricity.

4 Conclusions

NH_3 synthesis from N_2 and H_2O was investigated using an electrochemical setup featuring Ru/ Cs^+ /C catalysts, Pd alloy membrane cathodes, NaOH-KOH molten electrolytes, and Ni anodes operated at $250 \text{ }^\circ\text{C}$ and 1.0 MPa . This electrochemical setup was integrated with a refrigerated gas/liquid separator at $-75 \text{ }^\circ\text{C}$ to concentrate NH_3 and a recirculation pump for unreacted H_2 and N_2 . Without NH_3 separation and unreacted gas recirculation, apparent current efficiency for NH_3 formation was 32–20% for $10\text{--}100 \text{ mA cm}^{-2}$ at 1.0 MPa and $250 \text{ }^\circ\text{C}$, which was limited by the thermodynamic equilibrium limitation estimated to be 36%. To obtain products beyond chemical equilibrium, the most effective method is to use NH_3 separation and unreacted gas recirculation. Using this apparatus setup, an apparent current efficiency of 90% and a production rate of $320 \text{ nmol s}^{-1} \text{ cm}^{-2}$ for NH_3 production were achieved for 100 mA cm^{-2} at 1.0 MPa and $250 \text{ }^\circ\text{C}$.

The H_2 -TPD results showed a unique effect on hydrogen adsorption due to the addition of the Cs^+ compound. This result may provide a new perspective on NH_3 synthesis catalysts.

The current density and current efficiency of the electrochemical cell being studied have been confirmed to be suitable for scaling up to a system that can be integrated with wind and solar power generation. With the anticipated increase in surplus renewable energy, we hope that the development of such systems will be necessary in the future.

Data availability

Raw data were generated at Fukuoka University. Derived data supporting the findings of this study are available from the



corresponding author Jun Kubota on request. The data that support the findings of this study are available from the corresponding author, Jun Kubota, upon reasonable request.

Author contributions

Sagara was primarily involved in practical experimental studies and data analysis. Watanabe, along with Sagara, conducted TPD measurements and processed the data. Kubota played a multi-faceted role including supervision in this study.

Conflicts of interest

There are no conflicts to declare.

Acknowledgements

A part of this article is based on results obtained from a project, JPNP14004, “Highly-efficient NH₃ electrochemical synthesis technology from renewable energy electricity (FY2022-2023)”, commissioned by the New Energy and Industrial Technology Development Organization (NEDO), Japan.

References

- 1 I. Rafiqul, C. Weber, B. Lehmann and A. Voss, *Energy*, 2005, **30**, 2487–2504.
- 2 A. Valera-Medina, F. Amer-Hatem, A. K. Azad, I. C. Dedoussi, M. de Joannon, R. X. Fernandes, P. Glarborg, H. Hashemi, X. He, S. Mashruk, J. McGowan, C. Mounaim-Rouselle, A. Ortiz-Prado, A. Ortiz-Valera, I. Rossetti, B. Shu, M. Yehia, H. Xiao and M. Costa, *Energy Fuels*, 2021, **35**, 6964–7029.
- 3 R. F. Service, *Science*, 2018, **361**, 120–123.
- 4 *Ammonia: Catalysis and Manufacture*, ed. A. Nielsen, Springer-Verlag, Berlin, 1995.
- 5 International Energy Agency, *Ammonia Technology Roadmap*, 2021.
- 6 *CRC Handbook of Chemistry and Physics*, ed. J. Rumble, 99th edn, CRC Press, 2018.
- 7 I. Chorkendorff and J. W. Niemantsverdriet, *Concepts of Modern Catalysis and Kinetics*, Wiley-VCH, 2007.
- 8 H. Ishaq and C. Crawford, *Energy Convers. Manage.*, 2024, **300**, 117869.
- 9 U. Jafar, U. Nuhu, W. U. Khan and M. M. Hossain, *Int. J. Hydrogen Energy*, 2024, **71**, 857–876.
- 10 D. R. MacFarlane, P. V. Cherepanov, J. Choi, B. H. R. Suryanto, R. Y. Hodgetts, J. M. Bakker, F. M. F. Vallana and A. N. Simonov, *Joule*, 2020, **4**, 1186–1205.
- 11 S. Giddey, S. P. S. Badwal, C. Munnings and M. Dolan, *ACS Sustainable Chem. Eng.*, 2017, **6**, 10231–10239.
- 12 C. R. Santhosh and R. Sankannavar, *Appl. Energy*, 2023, **352**, 121960.
- 13 B. Wang, T. Li, F. Gong, M. H. D. Othman and R. Xiao, *Fuel Process. Technol.*, 2022, **235**, 107380.
- 14 G. Qing, R. Ghazfar, S. T. Jackowski, F. Habibzadeh, M. M. Ashtiani, C.-P. Chen, M. R. Smith III and T. W. Hamann, *Chem. Rev.*, 2020, **120**, 5437–5516.
- 15 A. J. Martín, T. Shinagawa and J. Pérez-Ramírez, *Chem*, 2019, **5**, 263–283.
- 16 X. Guo, Y. Zhu and T. Ma, *J. Energy Chem.*, 2017, **26**, 1107–1116.
- 17 S. Giddey, S. P. S. Badwal and A. Kulkarni, *Int. J. Hydrogen Energy*, 2013, **38**, 14576–14594.
- 18 I. A. Amar, R. Lan, C. T. G. Petit and S. Tao, *J. Solid State Electrochem.*, 2011, **15**, 1845–1860.
- 19 L. F. Greenlee, J. N. Renner and S. L. Foster, *ACS Catal.*, 2018, **8**, 7820–7827.
- 20 S. Z. Andersen, V. Čolić, S. Yang, J. A. Schwalbe, A. C. Nielander, J. M. McEnaney, K. Enemark-Rasmussen, J. G. Baker, A. R. Singh, B. A. Rohr, M. J. Statt, S. J. Blair, S. Mezzavilla, J. Kibsgaard, P. C. K. Vesborg, M. Cargnello, S. F. Bent, T. F. Jaramillo, I. E. L. Stephens, J. K. Nørskov and Ib Chorkendorff, *Nature*, 2019, **570**, 504–508.
- 21 A. Mangini, L. Fagiolari, A. Sacchetti, A. Garbujo, P. Biasi and F. Bella, *Adv. Energy Mater.*, 2024, **14**, 2400076.
- 22 N. Lazouski, Z. J. Schiffer, K. Williams and K. Manthiram, *Joule*, 2019, **3**, 1127–1139.
- 23 A. Tsuneto, A. Kudo and T. Sakata, *J. Electroanal. Chem.*, 1994, **367**, 183–188.
- 24 Y. Ito, T. Nishikiori and H. Tsujimura, *Faraday Discuss.*, 2016, **190**, 307–326.
- 25 C. A. Fernandez, N. M. Hortance, Y.-H. Liu, J. Lim, K. B. Hatzell and M. C. Hatzell, *J. Mater. Chem. A*, 2020, **8**, 15591–15606.
- 26 C. A. Fernandez and M. C. Hatzell, *J. Electrochem. Soc.*, 2020, **167**, 143504.
- 27 K. Imamura, M. Matsuyama and J. Kubota, *Chem. Select*, 2017, **2**, 11100–11103.
- 28 K. Imamura and J. Kubota, *Sustain. Ener. Fuels*, 2018, **2**, 1278–1286.
- 29 K. Imamura and J. Kubota, *Sustain. Ener. Fuels*, 2019, **3**, 1406–1417.
- 30 S. Nagaishi, R. Hayashi, A. Hirata, R. Sagara and J. Kubota, *Sustain. Ener. Fuels*, 2024, **8**, 914–926.
- 31 Y. Yuan, S. Tada and R. Kikuchi, *Sustain. Ener. Fuels*, 2022, **6**, 458–465.
- 32 Y. Yuan, S. Tada and R. Kikuchi, *Mater. Adv.*, 2021, **2**, 793–803.
- 33 N. Mohammad, A. B. Mohamad, A. A. H. Kadhum and K. S. Loh, *J. Power Sources*, 2016, **322**, 77–92.
- 34 T. Matsui, T. Kukino, R. Kikuchi and K. Eguchi, *J. Electrochem. Soc.*, 2006, **153**, A339–A342.
- 35 R. Sagara, R. Hayashi, A. Hirata, S. Nagaishi and J. Kubota, *Energy Adv.*, 2024, **3**, 1265–1270.
- 36 S. Licht, B. Cui, B. Wang, F.-F. Li, J. Lau and S. Liu, *Science*, 2014, **345**, 637–640.
- 37 S. Licht, B. Cui, B. Wang, F.-F. Li, J. Lau and S. Liu, Retraction, 14 Aug. 2020, *Science*, 2014, **345**, 637–640.
- 38 Y. Chen, H. Liu, N. Ha, S. Licht, S. Gu and W. Li, *Nature Catal.*, 2020, **3**, 1055–1061.
- 39 A. Ozaki and K. Aika, *Catalysis-Science and Technology*, ed. J. R. Anderson and M. Boudart, Springer-Verlag KG, Berlin, 1981, vol. 1, pp. 87–158.
- 40 K. Aika, *Catal. Today*, 2017, **286**, 14–20.



41 J. Kubota and K. Aika, *J. Phys. Chem.*, 1994, **98**, 11293–11300.

42 K. Aika, J. Kubota, Y. Kadowaki, Y. Niwa and Y. Izumi, *Appl. Surf. Sci.*, 1997, **121**, 488–491.

43 M. Kitano, Y. Inoue, Y. Yamazaki, F. Hayashi, S. Kanbara, S. Matsuishi, T. Yokoyama, S.-W. Kim, M. Hara and H. Hosono, *Nature Chem.*, 2012, **4**, 934–940.

44 Y. Ogura, K. Tsujimaru, K. Sato, S. Miyahara, T. Toriyama, T. Yamamoto, S. Matsumura and K. Nagaoka, *ACS Sustainable Chem. Eng.*, 2018, **6**, 17258–17266.

45 C. N. R. Rao and G. R. Rao, *Surf. Sci. Rep.*, 1991, **13**, 223–263.

46 K. Higuchi, H. Sugiyama and J. Kubota, *J. Phy. Chem. C*, 2017, **121**, 14581–14588.

47 H. Shinizu, K. Christmann and G. Ertl, *J. Catal.*, 1980, **61**, 412–429.

48 K. Christmann, *Surf. Sci. Rep.*, 1988, **9**, 1–163.

49 G. H. Rocker, C. L. Cobb, C.-S. Jun, H. Metiu and R. M. Martin, *Surf. Sci.*, 1989, **208**, 205–220.

50 Y. Kadowaki and K. Aika, *J. Catal.*, 1996, **161**, 178–185.

51 S. Miyahara, K. Sato, Y. Kawano, K. Imamura, Y. Ogura, K. Tsujimaru and K. Nagaoka, *Catal. Today*, 2021, **376**, 36–40.

52 Global Wind Energy Council (GWEC), Global Offshore Wind Report, 2024, <https://www.gwec.net/>.

53 International Energy Agency (IEA), Offshore Wind Outlook, 2019, <https://www.iea.org>.

